Science Bulletin 68 (2023) 2054–2062

Contents lists available at ScienceDirect

Science Bulletin

journal homepage: www.elsevier.com/locate/scib

Article

A smart thermal-gated bilayer membrane for temperature-adaptive radiative cooling and solar heating

Xinzhe Min [a,1], Xueyang Wang [a,1], Jinlei Li [a], Ning Xu [a], Xiran Du [a], Mengyue Zeng [a], Wei Li [b,*], Bin Zhu [a,*], Jia Zhu [a,*]

[a] National Laboratory of Solid State Microstructures, College of Engineering and Applied Sciences, Jiangsu Key Laboratory of Artificial Functional Materials, Collaborative Innovation Center of Advanced Microstructures, Nanjing University, Nanjing 210093, China
[b] GPL Photonics Laboratory, State Key Laboratory of Luminescence and Applications, Changchun Institute of Optics, Fine Mechanics and Physics, Chinese Academy of Sciences, Changchun 130033, China

ARTICLE INFO

Article history:
Received 26 February 2023
Received in revised form 2 June 2023
Accepted 28 July 2023
Available online 4 August 2023

Keywords:
Radiative cooling
Solar heating
Switchable Al_2O_3 NPs-composited PNIPAm hydrogel
Al_2O_3 nanoparticles
Temperature control

ABSTRACT

Due to the huge energy consumption of traditional cooling- and heating-based electricity, passive radiative cooling and solar heating with a minimum carbon footprint using the outer space and Sun as natural thermodynamic resources have attracted much attention. However, most passive devices are static and monofunctional, and cannot meet the practical requirements of dynamic cooling and heating under various conditions. Here, we demonstrate a smart thermal-gated (STG) bilayer membrane that enables fully automatic and temperature-adaptive radiative cooling and solar heating. Specifically, this device can switch from reflective to absorptive (white to black) in the solar wavelength with the reduction in optical scattering upon ambient temperature, corresponding to a sunlight reflectivity change from 0.962 to 0.059 when the temperature drops below ~30 °C, whereas its mid-infrared emissivity remains at ~0.95. Consequently, this STG membrane achieves a temperature of ~5 °C below ambient (a key signature of radiative cooling) under direct sunlight (peak solar irradiance >900 W m^{-2}) in summer and a solar heating power of ~550 W m^{-2} in winter. Theoretical analysis reveals the substantial advantage of this switchable cooling/heating device in potential energy saving compared with cooling-only and heating-only strategies when widely used in different climates. It is expected that this work will pave a new pathway for designing temperature-adaptive devices with zero energy consumption and provide an innovative way to achieve sustainable energy.

1. Introduction

Maintaining a relatively stable temperature plays a critical role in various industries, such as the breeding and brewing industries [1,2]. However, traditional temperature regulation mainly relies on air conditioning, which consumes a considerable amount of energy [3,4]. It has been reported that the energy consumption of indoor temperature regulation devices for heating and cooling accounts for 20% of the world's total energy demand, producing large amounts of carbon dioxide emissions [5,6]. Therefore, it is essential to develop energy-saving temperature regulation approaches with a minimum carbon footprint. In recent years, radiative cooling [7–22] using the outer space (3 K) as the cold source and solar heating [23–27] using the Sun (5800 K) as the heat source have been proposed to effectively realize passive cooling and heating without extra energy consumption (Fig. 1a). However, previously devices for radiative cooling or solar heating were mostly static or quasi dynamic, making it difficult to meet the dynamic cooling and heating demands to maintain a constant temperature.

Some efforts have been made to achieve switchable radiative cooling and solar heating [28–33]. For example, Zhao et al. [34] presented porous silicone coatings as platforms for optical management with reversible mechanical forces. Li et al. [35] demonstrated a dual-mode heat managing device that can switch radiative cooling and solar heating functions through a pair of rotary actuators or rollers. These strategies always require extra energy. However, as the requirements of heating or cooling depend on ambient temperature, it is desirable to develop a smart and precise temperature regulator triggered directly by temperature.

A few strategies have been demonstrated to achieve temperature-adaptive and passive radiative cooling and heating

* Corresponding authors.
E-mail addresses: weili1@ciomp.ac.cn (W. Li), binzhu@nju.edu.cn (B. Zhu), jiazhu@nju.edu.cn (J. Zhu).
[1] These authors contributed equally to this work.

https://doi.org/10.1016/j.scib.2023.08.003
2095-9273/

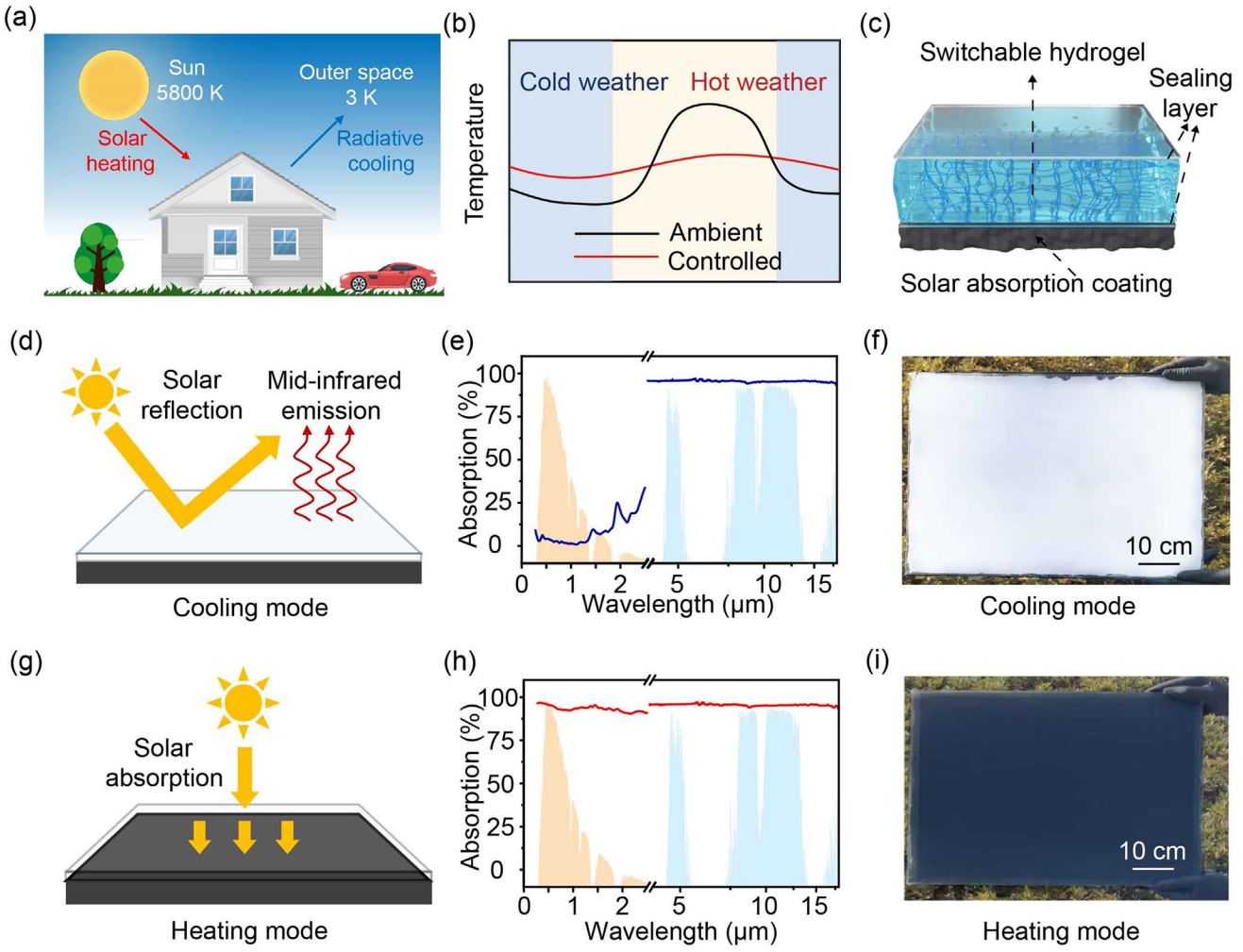

Fig. 1. (Color online) The design of the STG membrane. (a) Schematic of passive radiative cooling using the outer space (3 K) as the cold source and passive solar heating using the Sun (5800 K) as the heat source. (b) Concept of the ideal smart temperature control in summer and winter. The red line represents the temperature for ideal smart temperature control, and the black line represents ambient temperature in summer and winter. (c) Schematic of the STG membrane, which consists of a switchable hydrogel atop a solar absorption coating layer. (d) Schematic of the STG membrane in cooling mode due to high reflection in the solar wavelength and high emission in the mid-infrared wavelength. (e) Solar (left axis) and mid-infrared (right axis) absorption spectra of the STG membrane in cooling mode. (f) Photograph (50 cm × 70 cm) of the STG membrane in cooling mode. (g) Schematic of the STG membrane in heating mode due to high absorption in the solar wavelength. (h) Solar (left axis) and mid-infrared (right axis) absorption spectra of the STG membrane in heating mode. (i) Photograph (50 cm × 70 cm) of the STG membrane in heating mode.

[36–47]. For example, Tang et al. [48] developed temperature-adaptive radiative coating relying on thermotropic metal-insulator transition materials. Despite its ability to tune thermal emittance in response to ambient temperatures, it is incapable of regulating solar reflectivity/absorptivity to achieve solar heating. Fang et al. [49] realized a sandwich structure thermal homeostasiser based on thermochromic hydrogel, which achieved the switch between radiative cooling and solar heating. However, it is noted that a sub-ambient temperature under direct sunlight, the signature or the defining point for radiative cooling representing a net cooling power, has never been realized in all of those previous works.

In this work, we demonstrate a smart thermal-gated (STG) bilayer membrane that can automatically switch between radiative cooling and solar heating triggered by ambient temperature (Fig. 1b). This membrane comprises a thermoresponsive poly (N-isopropyl acrylamide) (PNIPAm) based hydrogel atop a reduced graphite oxide (rGO) coating layer (Fig. 1c). The top layer of the PNIPAm-based hydrogel can switch between transparent and reflective upon ambient temperature change, while the underlayer maximizes solar absorption. Specifically, when the temperature is above the low critical solution temperature (LCST) of the PNIPAm-based hydrogel, the top layer presents white, maximizing the backscattering of sunlight with solar reflectivity of 0.962. Meanwhile, the intrinsic molecular vibration modes of PNIPAm endow a high mid-infrared emissivity (0.95) in the 4–18 μm range (Fig. 1d–f), thus enabling excellent passive radiative cooling performance to decrease the temperature and achieve sub-ambient cooling. When the temperature is lower than the LCST, this bilayer membrane switches to heating mode. The top layer which becomes transparent, allows sunlight to pass through and be absorbed by the black rGO underlayer with solar absorption of 0.941 (Fig. 1g–i), thus enabling efficient passive solar heating performance to increase the temperature. Therefore, automatic switchable thermal properties are realized by this STG bilayer design based on passive radiative cooling and solar heating.

Leveraging this smart temperature-adaptive cooling/heating design, we experimentally observed that the inner temperature protected by the STG membrane was maintained around the LCST when the outer temperature switched from ~50 to ~0 °C. It can achieve up to ~100 W m^{-2} of cooling power at 50 °C and up to ~550 W m^{-2} of heating power at 15 °C. In addition, we model its

substantial advantage in energy potential compared with only radiative cooling and only solar heating strategies. It is expected that this design not only provides a new path for energy-saving building cooling/heating but also has implications in various other fields, such as fermentation and preservation of goods.

2. Materials and methods

2.1. Preparation of the STG membrane

The Al_2O_3 nanoparticles (NPs)-composited PNIPAm hydrogel was synthesized by the *in-situ* polymerization of the monomer in deionized water. First, 7.91 g (0.07 mol) of PNIPAm, 1.32 g (0.03 mol) of polyvinyl alcohol (PVA), and 215.6 mg (0.0014 mol) of *N*,*N*'-methylenebis (acrylamide) were dissolved in deionized water at 50 °C to make a homogenous 100 mL of the aqueous solution. Then, 10 mL of Al_2O_3 NPs (α phase) with a size of approximately 30 nm dispersion solution (20 g L^{-1} Al_2O_3 NPs, 12 g L^{-1} tetrabutyl titanate (TT)) was added to a 40 °C water bath for 1 h. After the homogeneous solution had been obtained, the temperature of the solution was reduced to room temperature (~25 °C), and the solution was purged with N_2 for 3 h. Subsequently, 1.35 mL of tetramethylethylenediamine (catalyst) and 2.7 mL of ammonium persulfate (initiator) were added in sequence to the solution with 30 s stirring. Last, the homogenous solution was injected between two clean glass slides, which had their edges pre-sealed with sealant before the experiment to make a sandwich structure. The sample is put at room temperature to stand for 24 h, the Al_2O_3 NPs-composited PNIPAm hydrogel with a thickness of ~500 μm was successfully made and sealed in glass slides. Graphene oxide (GO) nanosheets were dispersed in deionized water (3 mg mL^{-1}) by ultrasonic vibration for 2 h. Then, the GO solution was sprayed onto the preheated fabrics using a commercial airbrush to produce solar absorption GO-coated fabrics. The GO-coated fabrics were then baked at 150 °C in a vacuum to obtain solar absorption rGO-coated fabrics with a thickness of ~450 μm (Fig. S1 online). The as-prepared Al_2O_3 NPs-composited PNIPAm hydrogel and rGO-coated fabrics were tightly adhered by adding adhesives to their edges to form a double-layer STG membrane.

2.2. Preparation of the Al_2O_3 NPs-composited PNIPAm hydrogels with 30, 35, and 40 °C LCSTs

The LCST of PNIPAm hydrogel is mostly based on the hydrophilicity of the organic chain. Therefore, to control the LCST of the STG samples, we added 20% more PNIPAm to increase the length of the organic chain to enhance hydrophobicity during the fabrication process, and the LCST of the sample can be tuned to 30 °C. To increase the LCST, extra 20% PVA was added during the fabrication process to enhance the hydrophilicity of the sample. And the LCST can be precisely tuned to 40 °C. The LCST of the original PNIPAm hydrogel is 35 °C.

2.3. Material characterizations of the STG membrane

The microstructures of the PNIPAm-based hydrogel were characterized by an optical microscope (DS-FI2, Nikon). The microimages of the rGO coating were captured by scanning electron microscopy (SEM, MIRA3, TESCAN). A UV–Vis–NIR spectrophotometer (UV-3600, SHIMADZU) equipped with an integrating sphere (ISR-310) was used to measure the solar reflectivity spectra of samples. The mid-infrared emissivity spectra were measured with a Fourier transform infrared (FTIR) spectrophotometer (Nicolet iS50R, Thermo Fisher) equipped with an integrating sphere (4P-GPS-020-SL, Pike). The Raman spectra were obtained on MR350, SOL Instruments., Ltd.

2.4. Heating and cooling performance tests of the STG membrane

The heating and cooling temperature was monitored by K-type thermocouples. The heating/cooling load, a constant power, was applied by a semiconductor chilling plate/a Kapton heater with a temperature feedback circuit. The heating power was obtained by monitoring the cooling power of the semiconductor chilling plate with a power meter (66205, Chroma). The energy conversion efficiency of electrical power to semiconductor refrigeration power is ~50%. The cooling power was obtained by monitoring the heating power of the Kapton heater by a power meter (66205, Chroma), a mature method repeatedly used in Refs. [7,8,10]. The solar power was measured by a solar radiation meter (TBQ) or a portable solar power meter (1333R, TES Electrical Electronic Co.). Ambient temperature and relative humidity were monitored by a temperature and humidity recorder in a shelter (Tuolaisi Co., Ltd.) or a portable device (COS-03-5, Shandong Renke Control Technology Co., Ltd.).

3. Results and discussion

3.1. The design of the switchable Al_2O_3 NPs-composited hydrogel

As demonstrated above, the top layer with switchable optical properties is the most critical for this STG membrane. PNIPAm hydrogel, a thermoresponsive material that can switch its optical properties as temperature changes, is widely used in a series of applications, such as heat-sensitive coatings and smart windows [50–53]. The optical properties of PNIPAm hydrogel are fundamentally related to its porous network, which shrink when the temperature is beyond its LCST due to the formation of intramolecular hydrogen bonds inside the chains. This structural change induces its strong scattering of sunlight, from transparent (0.86) to reflective (0.83) (Fig. S2 online). Meanwhile, the main component of PNIPAm possesses high emissivity in the mid-infrared spectrum (8–13 μm), which can radiate heat. Therefore, PNIPAm can be considered as a promising candidate for radiative cooling when the temperature is beyond its LCST. However, according to previous results, for a radiative cooler to achieve sub-ambient cooling, over 90% of incident sunlight must be reflected [54]. To realize temperature control of the STG device, it is desirable to further increase the solar reflectivity of the original PNIPAm hydrogel without negatively affecting its thermal emission properties.

To increase the solar reflectivity of the PNIPAm hydrogel, we considered the mechanism of the switchable optical properties of the PNIPAm hydrogel. The PNIPAm molecules have a loose chain structure at low temperatures, and a huge amount of hydrogen bonds are formed between the hydrophilic groups on the chain and water molecules to maintain the stability of the structure. This structure can effectively allow light to pass through, thus showing high transmittance. When the temperature rises above the LCST, the hydrogen bond between the molecular chain and water molecules breaks. To reach a low-energy state, the molecular chain shrinks to form a close-packed island structure [53]. The island-shaped PNIPAm molecules can effectively scatter light, thereby exhibiting high reflectivity. The strong reflectivity of the PNIPAm hydrogel mainly derives from the difference in the refractive index between the organic phase (~1.49) and water (~1.33). According to the Mie scattering theory, increasing the difference of refractive index for the two phases can increase the solar reflectivity of the PNIPAm hydrogel. Here, we introduced Al_2O_3 NPs with a high refractive index (~1.8) and a size of approximately 30 nm in the organic phase chain structure to increase its refractive index. How-

ever, if Al_2O_3 NPs are added directly to the PNIPAm hydrogel, they disperse into the aqueous phase and cannot increase the scattering coefficient of the organic phase because Al_2O_3 NPs are hydrophilic. Inspired by the coupling reaction used in plasthetics [55,56], a coupling reagent called TT is chosen to connect Al_2O_3 NPs with the organic phase chain structure (PNIPAm/PVA). The butoxy group in TT can react directly with the hydroxyl group on the surface of Al_2O_3 via scission of one butoxy chain of TT, thus leading to chemical bonding with Al_2O_3. The same reaction also occurs between TT and the PVA chain of the organic phase [57]. Therefore, strong bonds and good adhesion between Al_2O_3 NPs and organic phases are formed by this molecular-designed bonding (Fig. 2a).

The Raman spectra results confirm that Al_2O_3 NPs only exist inside and the boundary of the organic phase after phase separation due to the strong bond between organic phase chain structure and Al_2O_3 NPs (Fig. 2b and Fig. S3 online). The organic phase of the Al_2O_3 NPs-composited PNIPAm hydrogel has a significantly increased effective refractive index from 1.49 to 1.69, resulting in higher solar reflectance. We also calculated the scattering efficiency of the organic phase island as a function of the sizes across the solar spectrum (0.28–2.5 μm) using the Mie scattering theory. Strong scattering in the solar spectrum can be achieved for island sizes between 5 and 20 μm (Fig. 2c), and thus we adjusted the size of the organic island by refining the scattering point in this range (Fig. S4 online). Fig. 2d shows the solar reflectivity of the Al_2O_3 NPs-composited PNIPAm hydrogel in cooling mode, with a significantly improved reflectivity of ~0.962 in the solar wavelength (0.28–2.5 μm), ideal for sub-ambient daytime radiative cooling. Meanwhile, the Al_2O_3 NPs-composited PNIPAm hydrogel maintained a solar transmittance of 0.9 in heating mode (Fig. S5 online). In addition, we have applied a radical polymerization, spraying and annealing synthesis method, which has shown potential for scaling up to realize the aforementioned tandem STG membrane.

It is important to precisely control various temperature ranges for practical applications. It can be seen from the COMSOL simulation that a controlled temperature is always established

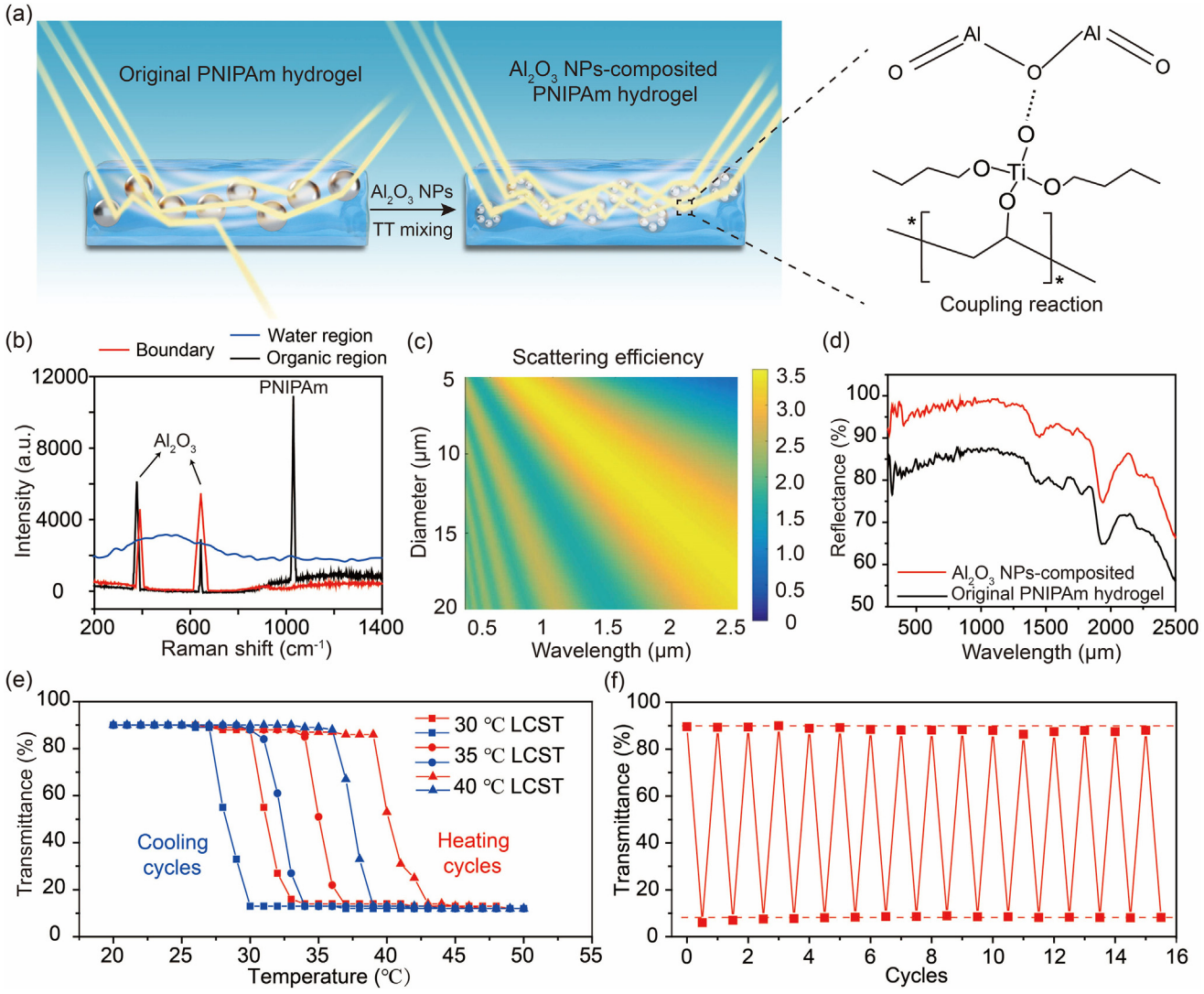

Fig. 2. (Color online) Structures and characterizations of the Al_2O_3 NPs-composited PNIPAm hydrogel. (a) Schematic of the fabrication for the Al_2O_3 NPs-composited PNIPAm hydrogel. TT as a coupling reagent to facilitate the bonding of Al_2O_3 NPs to the PVA chain of organic phase through a coupling reaction. The asterisks represent other chain structures. (b) The Raman spectra of various regions in the Al_2O_3 NPs-composited PNIPAm hydrogel, including the boundary of the organic phase, inside the organic phase and inside the water phase. (c) Simulation of scattering efficiency of the organic phase island in the Al_2O_3 NPs-composited PNIPAm hydrogel over the wavelength range of 0.28–2.5 μm, with the diameter of the size varying from 5 to 20 μm. (d) The reflectivity of the Al_2O_3 NPs-composited PNIPAm hydrogel and original PNIPAm hydrogel in the solar spectrum (0.28–2.5 μm). (e) The solar transmittance of 30, 35, and 40 °C LCST Al_2O_3 NPs-composited PNIPAm hydrogels between 20 and 50 °C showing the temperature-adaptive switching. (f) The solar transmittance of the Al_2O_3 NPs-composited PNIPAm hydrogel in cycles. After 15 times of cycles between 50 and 25 °C, the solar transmittance of the STG membrane above LCST and below LCST had no significant decline.

around the LCST of the Al_2O_3 NPs-composited PNIPAm hydrogel under near-ideal conditions (Fig. S6, Note S1 and Table S1 online). Therefore, the precise modulation of the LCST of the Al_2O_3 NPs-composited PNIPAm hydrogel is a promising approach to tuning the temperature-control performance of space. By adjusting the hydrophilicity of PNIPAm chains with introduced different amounts of PVA and PNIPAm in the Al_2O_3 NPs-composited PNIPAm hydrogel [56], we can easily adjust the LCST of the Al_2O_3 NPs-composited PNIPAm hydrogel (see details in Methods). As shown in Fig. 2e, the solar transmittance of the fabricated Al_2O_3 NPs-composited PNIPAm hydrogels with LCSTs of 30, 35, and 40 °C can change around LCSTs in the heating and cooling cycles. Notably, the solar transmittance of the Al_2O_3 NPs-composited PNIPAm hydrogel in two modes maintains stable over 15 times cycles time (Fig. 2f). It is noted that the Al_2O_3 NPs-composited PNIPAm hydrogel also performs stable optical performance outdoors (Fig. S7 online).

3.2. The temperature regulation of the STG membrane

To examine the temperature regulation of the STG membrane, we used a nested device to create controlled experimental conditions for the outdoor tests (Fig. 3a and c). The device has several parts, including an inside container that is covered by an insulation layer and takes the role of a protected object, an outside container that can hold hot water/ice to create hot/cold conditions, and a 30 °C LCST STG membrane on the top to manipulate the temperature of the inside container. Here, a thermal insulator (containers protected by a pure insulation membrane) is set as the control group. We tested the cooling performance of the STG membrane

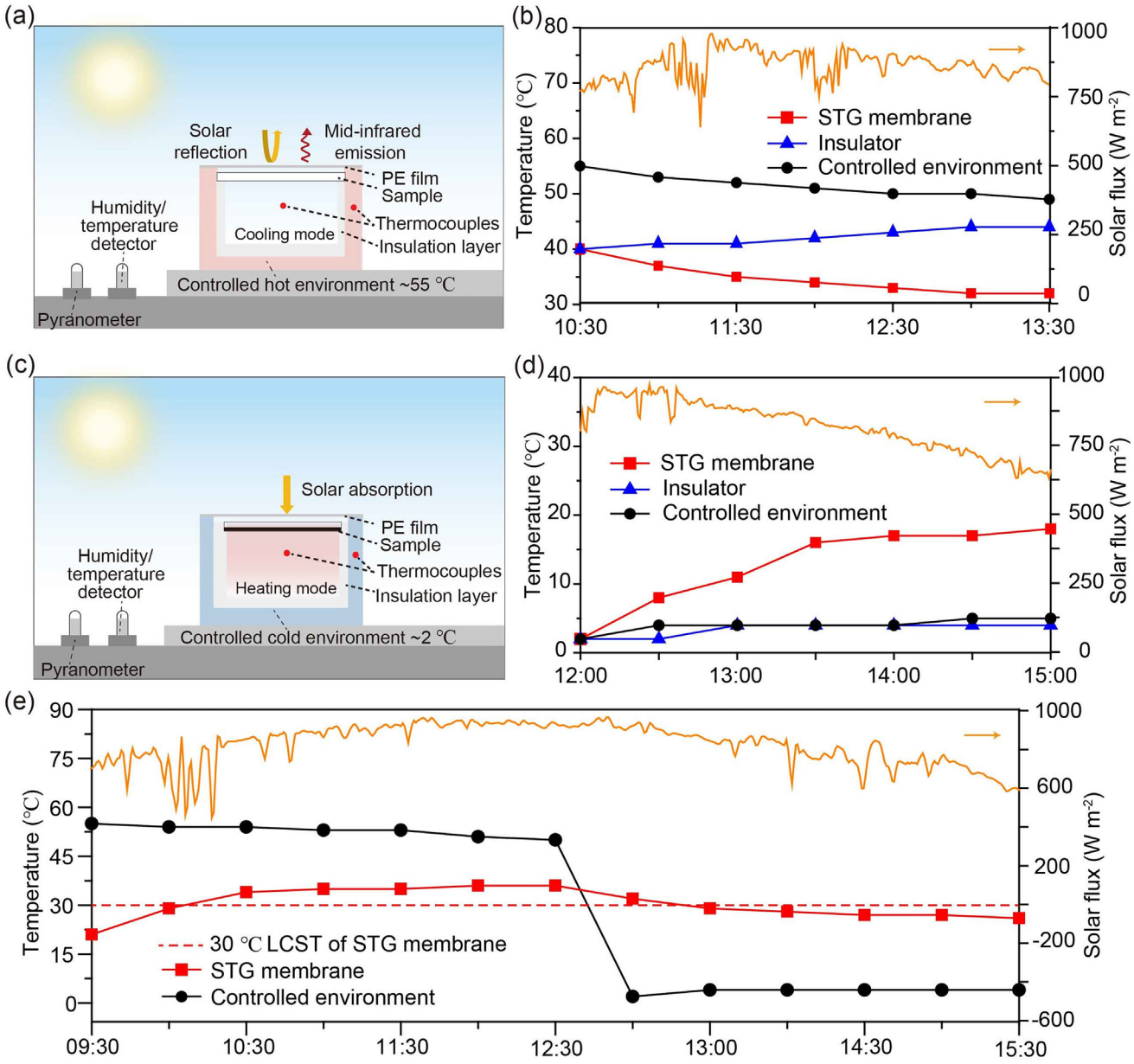

Fig. 3. (Color online) The temperature regulation of the STG membrane under controlled hot/cold conditions. (a) Schematic of the device creating a controlled hot environment for cooling performance tests. (b) Power of incident sunlight and the temperature control performance of the STG membrane in a hot environment. (c) Schematic of the device creating a controlled cold environment for heating performance tests. (d) Power of incident sunlight and the temperature control performance of the STG membrane in a cold environment. (e) Power of incident sunlight and the temperature control performance of the STG membrane in alternating hot and cold environments.

in a 55 °C hot environment, wherein the STG membrane effectively lower the inner temperature from 40 °C to approximately 32 °C, close to the LCST (30 °C) of the STG membrane (Fig. 3b). In contrast, the temperature of the thermal insulator continuously increased to approximately 45 °C with a mean sunlight irradiance of ~800 W m^{-2} (ambient conditions shown in Fig. S8 online). When switching to heating mode in a ~2 °C cold environment, the temperature of the inner side of the container quickly rises to approximately 24 °C within 3 h (approaching the LCST of the STG membrane, Fig. 3d), while the temperature of the insulator-protecting container remains ~2 °C with a mean sunlight irradiance of ~700 W m^{-2} (Fig. S9 (online) for ambient conditions). Even in alternating hot and cold environments, the STG membrane also exhibits excellent temperature control performance. As shown in Fig. 3e, with an initial temperature of 20 °C, the 30 °C LCST STG membrane can effectively control the temperature inside the container to approximately 30 °C, with a temperature difference of less than 5 °C, regardless of the outer temperature changes (from ~50 to ~0 °C) with ambient conditions shown in Fig. S10 (online). The temperature difference is mainly due to the unavoidable conductive heat changes between the inside and outside containers. This experimental result further verifies that the STG membrane shows excellent temperature control performance under various working conditions.

3.3. The cooling/heating performance of the STG membrane in practical outdoor conditions

As solar heating/radiative cooling power is a common and crucial factor to evaluate the heating/cooling performance, we performed an outdoor measurement of the heat flux of the STG membrane in practical outdoor conditions via the setup shown in Fig. 4a. The positive heat flux represents net heating power, and the negative flux represents net cooling power. We tested the heating and cooling power of the STG membrane with the temperature slowly rising from 15 to 50 °C (the corresponding ambient conditions during measurements are presented in Figs. S11–S14 online). As shown in Fig. 4b, the heating power reached 550, 400, and 300 W m^{-2} at 15, 20, and 25 °C, respectively. When the temperature reached the LCST (30 °C), the STG membrane automatically switched to cooling mode. The average net cooling power of the STG membrane reached 52, 70, 90, and 100 W m^{-2} at 35, 40, 45, and 50 °C, respectively. The results clearly indicate the excellent switchable cooling/heating performance of our designed STG membrane.

We further tested the cooling/heating temperature performance of the STG membrane in practical outdoor conditions. As shown in Fig. 4c–e and Fig. S15 (online), in hot weather with an ambient temperature of ~35 °C, the STG membrane induced a sub-ambient temperature drop of ~5 °C under direct sunlight (peak solar irradiance > 900 W m^{-2}). Furthermore, even in the absence of insulated conditions, this STG membrane achieves a temperature of ~0.6 °C below ambient under direct sunlight exceeding 900 W m^{-2} (Fig. S16 online). When placed in cold weather, it converted to heating mode, the STG membrane achieves a neat increase of a maximum of 8 °C from 11:00 am to 2:00 pm under an average solar irradiance of ~600 W m^{-2} at an ambient temperature of ~20 °C (Fig. 4f–h, Fig. S17 and Table S2 online). It illustrates that the STG membrane shows an effective practical heating/cooling effect in winter/summer.

3.4. The energy potential simulation

To quantitively predict the potential impact of our STG membrane on energy-saving, we developed a thermal model (more details about calculation can be found in Note S2 in the Supplementary materials) with optical properties of material and real weather data to calculate the monthly (winter: December, January, February, and summer: the daytime average temperature is above 30 °C) energy potential for only solar heating, only radiative cool-

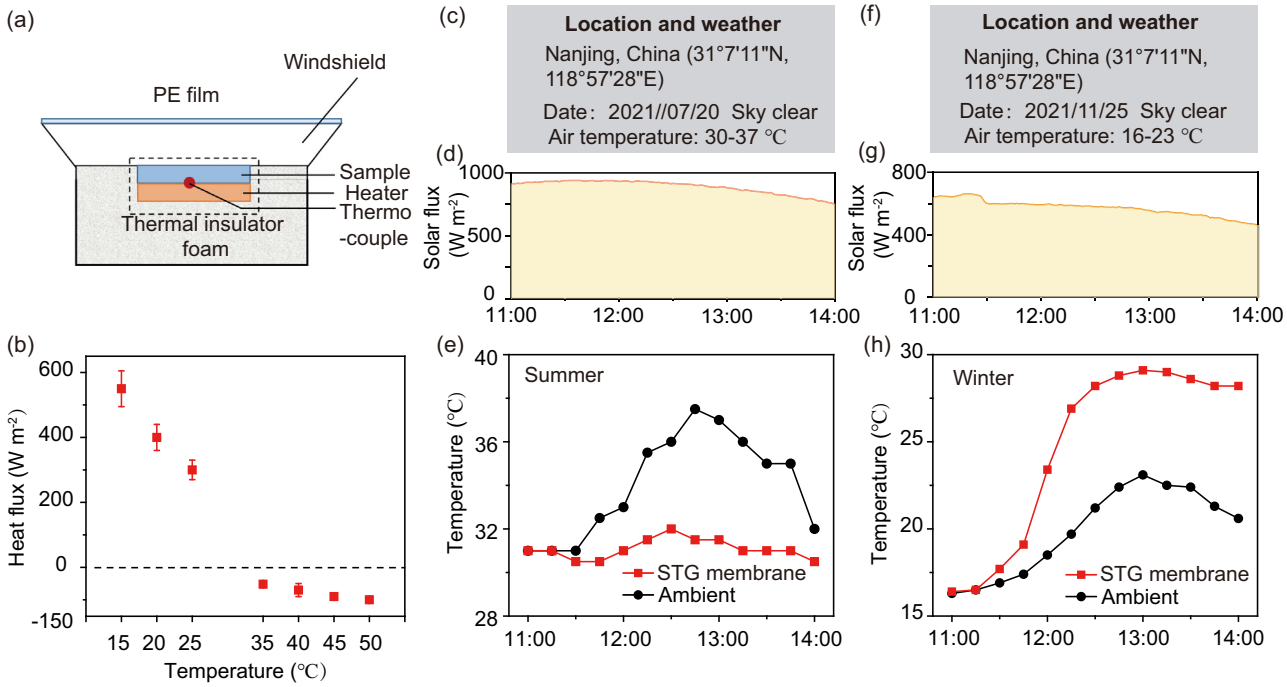

Fig. 4. (Color online) Outdoor real-time cooling/heating performance of the STG membrane. (a) Schematic of the device for the heat flux and cooling/heating temperature test. (b) Switchable heating and cooling powers of the STG membrane when the controlled temperature changes. (c) Topographic and meteorological information of the location of the cooling temperature performance test in summer. (d) Power of incident sunlight and (e) cooling performance of STG membrane in hot weather (summer). (f) Topographic and meteorological information of the location of the heating temperature performance test in winter. (g) Power of incident sunlight and (h) heating performance of the STG membrane in cold weather (winter).

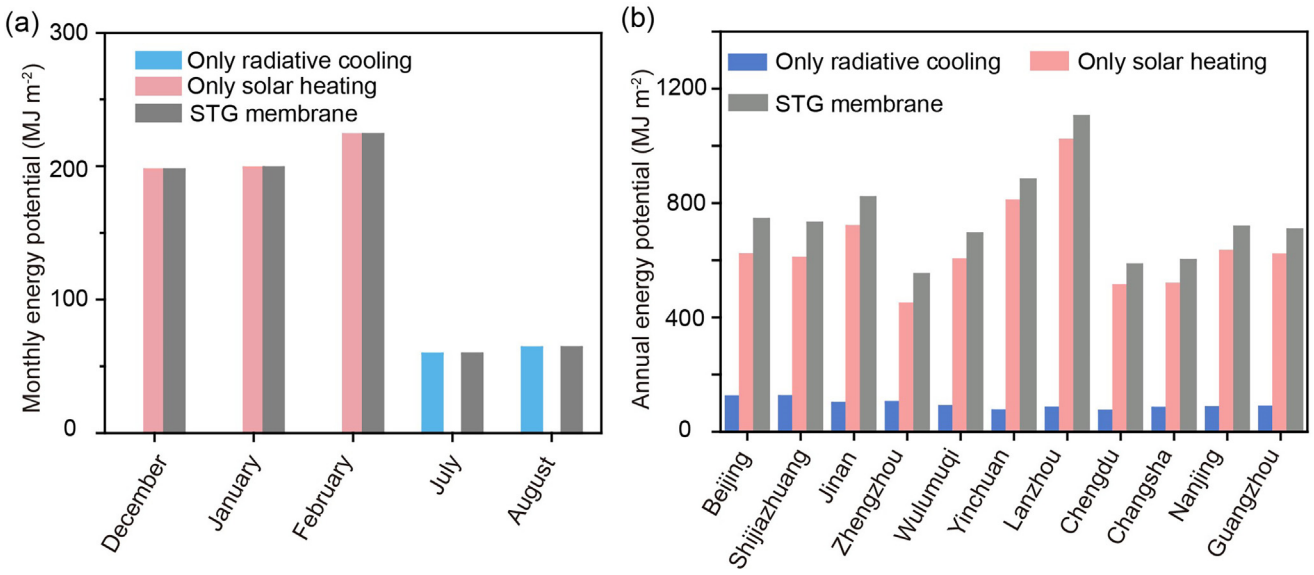

Fig. 5. (Color online) Modeled energy potential of different energy-saving modes. (a) Monthly energy potential with different modes in Beijing. (b) Annual energy potential at different modes over 11 cities in different climates.

ing, and the STG membrane in Beijing (Fig. 5a). To be expected, only radiative cooling produced positive energy potential in summer. And only solar heating could save notable energy in winter. However, the STG membrane achieved positive energy potential in both summer and winter. Quantitatively, the total annual energy potential of the STG membrane is 6 times and 1.2 times more than the only radiative cooling and only solar heating in Beijing, respectively. Annual energy potentials were also calculated for additional 11 cities in different climates, including temperate monsoon (Beijing, Shijiazhuang, Jinan, Zhengzhou), temperate steppe/desert (Wulumuqi, Yinchuan, Lanzhou), and subtropical (Chengdu, Changsha, Nanjing, Guangzhou) climates. It is obvious that the STG membrane shows a remarkable energy-potential performance under different climates, compared with single-mode devices (Fig. 5b).

We also experimentally verified that the STG membrane is suitable for maintaining the temperature of alcohol fermentation. Compared with the container by electric heating and unprotected container, the temperature of the container protected by the STG membrane was closer to the appropriate temperature of alcohol fermentation (30–35 °C). And after six days, the STG membrane-protected container generated the highest concentration of alcohol with zero energy consumption (Fig. S18 online).

4. Conclusion

In summary, we experimentally demonstrated that passive solar heating and radiative cooling can be integrated into the STG membrane composed of an Al_2O_3 NPs-composited PNIPAm hydrogel atop an rGO layer with switchable optical properties upon temperature change. With the molecular surface treatment, this STG membrane can switch from reflective to absorptive with the solar reflectivity change from 0.962 to 0.059, enabling the system from the radiative cooling mode at high temperatures to solar heating at low temperatures. Outdoor experimental results and theoretical analysis both demonstrate the precise temperature control and the advantage in energy-saving of this STG membrane. We expect that it will inspire more innovative designs for advanced smart temperature control materials and devices toward an energy-efficient and sustainable society.

Conflict of interest

The authors declare that they have no conflict of interest.

Acknowledgments

We acknowledge the Micro-fabrication Center at the National Laboratory of Solid State Microstructures (NLSSM) for technical support. Jia Zhu acknowledges the support from the XPLORER PRIZE. This work was jointly supported by the National Key Research and Development Programme of China (2022YFA1404704 and 2020YFA0406104), the National Natural Science Foundation of China (52002168, 12022403, 11874211, 62134009, 62121005, and 61735008), Excellent Research Programme of Nanjing University (ZYJH005), the Fundamental Research Funds for the Central Universities (021314380184, 021314380208, 021314380190, 021314380140, and 021314380150), and State Key Laboratory of New Textile Materials and Advanced Processing Technologies (Wuhan Textile University, No. FZ2022011).

Author contributions

Bin Zhu, Xinzhe Min, Xueyang Wang, and Jia Zhu conceived and planned this research. Xinzhe Min, Xueyang Wang, Xiran Du, and Jinlei Li did the experiments. Wei Li contributed to the optical modeling and thermal analysis. Xueyang Wang performed the energy potential simulation. Xinzhe Min, Xueyang Wang, Bin Zhu, Mengyue Zeng, Ning Xu, and Jia Zhu organized the data and wrote the manuscript. All authors discussed the results and approved the final version of the manuscript.

Appendix A. Supplementary materials

Supplementary materials to this article can be found online at https://doi.org/10.1016/j.scib.2023.08.003.

References

[1] Chakraborty S, Newton AC. Climate change, plant diseases and food security: an overview. Plant Pathol 2011;60:2–14.

[2] Mun SG. The effects of ambient temperature changes on foodborne illness outbreaks associated with the restaurant industry. Int J Hosp Manage 2020;85:102432.
[3] Chu S, Majumdar A. Opportunities and challenges for a sustainable energy future. Nature 2012;488:294–303.
[4] Burke M, Hsiang SM, Miguel E. Global non-linear effect of temperature on economic production. Nature 2015;527:235–9.
[5] Florides GA, Tassou SA, Kalogirou SA, et al. Review of solar and low energy cooling technologies for buildings. Renew Sustain Energy Rev 2002;6:557–72.
[6] Pérez-Lombard L, Ortiz J, Pout C. A review on buildings energy consumption information. Energy Build 2008;40:394–8.
[7] Zhu B, Li W, Zhang Q, et al. Subambient daytime radiative cooling textile based on nanoprocessed silk. Nat Nanotechnol 2021;16:1342–8.
[8] Raman AP, Anoma MA, Zhu L, et al. Passive radiative cooling below ambient air temperature under direct sunlight. Nature 2014;515:540–4.
[9] Li D, Liu X, Li W, et al. Scalable and hierarchically designed polymer film as a selective thermal emitter for high-performance all-day radiative cooling. Nat Nanotechnol 2021;16:153–8.
[10] Mandal J, Fu Y, Overvig AC, et al. Hierarchically porous polymer coatings for highly efficient passive daytime radiative cooling. Science 2018;362:315–9.
[11] Li T, Zhai Y, He S, et al. A radiative cooling structural material. Science 2019;364:760–3.
[12] Li J, Liang Y, Li W, et al. Protecting ice from melting under sunlight via radiative cooling. Sci Adv 2022;8:eabj9756.
[13] Wang X, Zhang Q, Wang S, et al. Sub-ambient full-color passive radiative cooling under sunlight based on efficient quantum-dot photoluminescence. Sci Bull 2022;67:1874–81.
[14] Zhou L, Song H, Liang J, et al. A polydimethylsiloxane-coated metal structure for all-day radiative cooling. Nat Sustain 2019;2:718–24.
[15] Li J, Wang X, Liang D, et al. A tandem radiative/evaporative cooler for weather-insensitive and high-performance daytime passive cooling. Sci Adv 2022;8:eabq0411.
[16] So S, Yang Y, Son S, et al. Highly suppressed solar absorption in a daytime radiative cooler designed by genetic algorithm. Nanophotonics 2021;11:2107–15.
[17] Chae D, Kim M, Lim H, et al. Selectively emissive fluoropolymer film for passive daytime radiative cooling. Opt Mater 2022;128:112273.
[18] Kim M, Lee D, Son S, et al. Visibly transparent radiative cooler under direct sunlight. Adv Opt Mater 2021;9:2002226.
[19] So S, Lee D, Badloe T, et al. Inverse design of ultra-narrowband selective thermal emitters designed by artificial neural networks. Opt Mater Express 2021;11:1863–73.
[20] Chae D, Lim H, So S, et al. Spectrally selective nanoparticle mixture coating for passive daytime radiative cooling. ACS Appl Mater Interfaces 2021;13:21119–26.
[21] Lee D, Go M, Son S, et al. Sub-ambient daytime radiative cooling by silica-coated porous anodic aluminum oxide. Nano Energy 2021;79:105426.
[22] Ko B, Lee D, Badloe T, et al. Metamaterial-based radiative cooling: towards energy-free all-day cooling. Energies 2018;12:89.
[23] Weinstein LA, Loomis J, Bhatia B, et al. Concentrating solar power. Chem Rev 2015;115:12797–838.
[24] Xu N, Zhang H, Lin Z, et al. A scalable fish-school inspired self-assembled particle system for solar-powered water-solute separation. Natl Sci Rev 2021;8:nwab065.
[25] Wang X, Lin Z, Gao J, et al. Solar steam-driven membrane filtration for high flux water purification. Nat Water 2023;1:391–8.
[26] Li X, Xu W, Tang M, et al. Graphene oxide-based efficient and scalable solar desalination under one sun with a confined 2D water path. Proc Natl Acad Sci USA 2016;113:13953–8.
[27] Zhou L, Tan Y, Wang J, et al. 3D self-assembly of aluminium nanoparticles for plasmon-enhanced solar desalination. Nat Photonics 2016;10:393–8.
[28] Hsu P-C, Liu C, Song AY, et al. A dual-mode textile for human body radiative heating and cooling. Sci Adv 2017;3:e1700895.
[29] Liu J, Zhou Z, Zhang D, et al. Research on the performance of radiative cooling and solar heating coupling module to direct control indoor temperature. Energy Convers Manage 2020;205:112395.
[30] Ono M, Chen K, Li W, et al. Self-adaptive radiative cooling based on phase change materials. Opt Express 2018;26:A777–87.
[31] Rao Y, Dai J, Sui C, et al. Ultra-wideband transparent conductive electrode for electrochromic synergistic solar and radiative heat management. ACS Energy Lett 2021;6:3906–15.
[32] Zhao X, Aili A, Zhao D, et al. Dynamic glazing with switchable solar reflectance for radiative cooling and solar heating. Cell Rep Phys Sci 2022;3:100853.
[33] Mandal J, Jia M, Overvig A, et al. Porous polymers with switchable optical transmittance for optical and thermal regulation. Joule 2019;3:3088–99.
[34] Zhao H, Sun Q, Zhou J, et al. Switchable cavitation in silicone coatings for energy-saving cooling and heating. Adv Mater 2020;32:2000870.
[35] Li X, Sun B, Sui C, et al. Integration of daytime radiative cooling and solar heating for year-round energy saving in buildings. Nat Commun 2020;11:6101.
[36] Zhang Q, Lv Y, Wang Y, et al. Temperature-dependent dual-mode thermal management device with net zero energy for year-round energy saving. Nat Commun 2022;13:4874.
[37] Shi M, Song Z, Ni J, et al. Dual-mode porous polymeric films with coral-like hierarchical structure for all-day radiative cooling and heating. ACS Nano 2023;17:2029–38.
[38] Liao M, Banerjee D, Hallberg T, et al. Cellulose-based radiative cooling and solar heating powers ionic thermoelectrics. Adv Sci 2023;10:2206510.
[39] Yang P, He J, Ju Y, et al. Dual-mode integrated janus films with highly efficient NAH_2PO_2-enhanced infrared radiative cooling and solar heating for year-round thermal management. Adv Sci 2023;10:2206176.
[40] Fei J, Han D, Ge J, et al. Switchable surface coating for bifunctional passive radiative cooling and solar heating. Adv Funct Mater 2022;32:2203582.
[41] Dai B, Li X, Xu T, et al. Radiative cooling and solar heating janus films for personal thermal management. ACS Appl Mater Interfaces 2022;14:18877–83.
[42] Mei X, Wang T, Chen M, et al. A self-adaptive film for passive radiative cooling and solar heating regulation. J Mater Chem A 2022;10:11092–100.
[43] Wang T, Zhang Y, Chen M, et al. Scalable and waterborne titanium-dioxide-free thermochromic coatings for self-adaptive passive radiative cooling and heating. Cell Rep Phys Sci 2022;3:100782.
[44] Ao X, Li B, Zhao B, et al. Self-adaptive integration of photothermal and radiative cooling for continuous energy harvesting from the sun and outer space. Proc Natl Acad Sci USA 2022;119:e2120557119.
[45] Kim M, Lee D, Yang Y, et al. Switchable diurnal radiative cooling by doped VO_2. Opto-Electron Adv 2021;4:200006.
[46] Wang S, Jiang T, Meng Y, et al. Scalable thermochromic smart windows with passive radiative cooling regulation. Science 2021;374:1501–4.
[47] Zhang Q, Wang Y, Lv Y, et al. Bioinspired zero-energy thermal-management device based on visible and infrared thermochromism for all-season energy saving. Proc Natl Acad Sci USA 2022;119:e2207353119.
[48] Tang K, Dong K, Li J, et al. Temperature-adaptive radiative coating for all-season household thermal regulation. Science 2021;374:1504–9.
[49] Fang Z, Ding L, Li L, et al. Thermal homeostasis enabled by dynamically regulating the passive radiative cooling and solar heating based on a thermochromic hydrogel. ACS Photonics 2021;8:2781–90.
[50] Tian J, Peng H, Du X, et al. Hybrid thermochromic microgels based on UCNPs/PNIPAm hydrogel for smart window with enhanced solar modulation. J Alloy Compd 2021;858:157725.
[51] Wei G, Yang D, Zhang T, et al. Thermal-responsive PNIPAm-acrylic/Ag NRs hybrid hydrogel with atmospheric window full-wavelength thermal management for smart windows. Sol Energy Mater Sol Cells 2020;206:110336.
[52] Haq MA, Su Y, Wang D. Mechanical properties of PNIPAm based hydrogels: A review. Mater Sci Eng C 2017;70:842–55.
[53] Liu J, Jiang L, He S, et al. Recent progress in PNIPAM-based multi-responsive actuators: A mini-review. Chem Eng J 2021;433:133496.
[54] Rephaeli E, Raman A, Fan S. Ultrabroadband photonic structures to achieve high-performance daytime radiative cooling. Nano Lett 2013;13:1457–61.
[55] Corbet J-P, Mignani G. Selected patented cross-coupling reaction technologies. Chem Rev 2006;106:2651–710.
[56] Tang L, Wang L, Yang X, et al. Poly (N-isopropylacrylamide)-based smart hydrogels: design, properties and applications. Prog Mater Sci 2021;115:100702.
[57] Zhou Y, Cai Y, Hu X, et al. Temperature-responsive hydrogel with ultra-large solar modulation and high luminous transmission for "smart window" applications. J Mater Chem A 2014;2:13550–5.

Xinzhe Min is a Ph.D. candidate at College of Engineering and Applied Science, Nanjing University. His research interest includes solar energy conversion, solar steam engine, radiative cooling and clean water generation.

Xueyang Wang is a Ph.D. candidate at College of Engineering and Applied Science, Nanjing University. Her research interest includes atmospheric water harvesting, interfacial solar-driven water generation, radiative cooling and photo-thermal energy conversion.

Wei Li received his Bachelor's degree from the Honors School at Harbin Institute of Technology (2011) and his Ph.D. degree from Vanderbilt University (2016). He was a postdoctoral fellow at Stanford University, working with Prof. Shanhui Fan. He is now a professor at Changchun Institute of Optics, Fine Mechanics and Physics (CIOMP), Chinese Academy of Sciences. He also serves as the director of GPL Photonics Laboratory at CIOMP. His research interest focuses on thermal photonics and energy applications including radiative cooling and solar energy harvesting.

Bin Zhu is an associate professor at College of Engineering and Applied Science, Nanjing University. He studied Materials Science and received his M.S. and Ph.D. degrees from Nanjing University. His research interest includes thermal management, radiative cooling and lithium battery.

Jia Zhu is a professor at College of Engineering and Applied Science, Nanjing University. He studied Physics at Nanjing University and received his M.S. and Ph.D. degrees in Electrical Engineering from Stanford University. Then he worked as a postdoctoral fellow at University of California, Berkeley and Lawrence Berkeley National Laboratory. In 2013, he returned back to Nanjing University, to be a professor at College of Engineering and Applied Sciences. His research interest is in the area of nanomaterials, nanophotonics and nanoscale heat transfer.